EFFECTS OF SLIP AND SIDE-SLIP ON T-CVTS PERFORMANCE AT URBAN CYCLE

Breno Raizer, breno_raizer@hotmail.com
Franco Giuseppe Dedini, dedini@fem.unicamp.br
DPM - FEM - UNICAMP

Abstract. *The automotive application of Continuously Variable Transmissions (CVTs) has been growing year after year. The reason is that CVTs allow a fuel consumption and pollutants emission reduction by optimizing the Internal Combustion Engine (ICE) operation. Other than that, CVTs have advantages concerning the automobile user comfort and noise reduction. The objective of this work is to develop a proposed methodology of optimization for Toroidal CVTs (T-CVTs) in automotive application. In this sense, the mathematical model was developed to evaluate the impact of variations in geometric parameters on the T-CVTs performance. These variations allow a verification of its influence on the system lifetime, torque capacity and efficiency for any urban cycle. New geometric parameters, related to the control system, were added to the T-CVTs basic geometric model. The purpose was to evaluate the Side-Slip along with Spin and Slip effects predicted by the elasto-hydrodynamic lubrication model (EHL) adopted. The results indicate that any misalignment of the power-rollers has a negative impact on the performance of the toroidal transmission.*

Keywords*: Toroidal CVT, simulation, urban cycle, optimization, life models*

1. INTRODUCTION

The growing request for pollutants emission reduction and higher energy efficiency has encouraged research on alternative technical solutions to improve the performance of nowadays Internal Combustion Engine (ICE) vehicles. Until renewable forms of energy become cost reasonable and effective, drive train systems equipped with continuously variable transmissions (CVTs) are being investigated for this purpose (Carbone *et al.*, 2004). CVTs seems to be relative costly in comparison to automatic transmissions (Tenberge & Möckel, 2002). But important benefits of using CVTs include fuel savings, reduced exhaust emissions, smooth power delivery, noise reduction, comfort and flexibility of application (Nikas, 2002).

The toroidal-type CVT (T-CVT) presents high efficiency and torque transmission capability, and among the many layouts of CVTs, a dual-cavity Half Toroidal CVT (HT-CVT) is found to be appropriate for automotive powertrain applications (Zhang *et al.*, 2000). Moreover the particular geometry of the toroidal traction drive makes it able to rapidly adjust its speed ratio to the request of the driver, thus improving the driving comfort (Carbone *et al.*, 2004). Torque is transmitted through Elasto-Hydrodynamic (EHD) fluid films between the contact surfaces of the input disk, the output disk and the power roller that is pressed between the two disks. Transmission Ratio (TR) change is achieved by tilting the angle of the power roller axis with respect to the disk axis.

Since durability, torque capacity and control of the power roller tilting angle are the key technical issues in the development of T-CVTs and their final cost (Zhang *et al.*, 2000), this paper reports on the results of theoretical modeling of a HT-CVT incorporated in a popular vehicle powertrain. In order to analyze the impact of possible misalignments in the T-CVTs performance, a new geometrical model were used together with a full EHD modeling, predicting effects like Slip and Side-Slip.

2. MATHEMATICAL MODEL OF T-CVT

The mathematical model used to simulate a T-CVT behavior is divided in three parts: modeling of system geometry, torque transmission and peripheral systems. The geometric model must provide for possible misalignment in the rollers axes in order to contemplate the effects of Side-slip, as well of Slip and Spin. The torque transmission model must predict the Elasto-Hydrodynamic (EHD) behavior of the lubrication fluid in the contact area, relating components surface velocities and pressure profile in contact area with the tangential forces transmitted. The modeled peripheral systems include the Loading Cam, responsible for the system pressurization, and a model to predict the bearing losses.

Figure 1 illustrates the basic geometry of a toroidal transmission. A T-CVT is composed of three main components: input disk, power roller and output disk. The space formed between the input and output discs is called toroidal cavity. For higher torque capacity, two or more rollers per cavity may be used, as well additional cavities (Zhang *et al.*, 2000). As shown in the Fig.1, the dimension and geometry of the T-CVT are defined by the Cavity Radius (R), Torus Radius (Y_0), Half-cone Angle (γ), Roller Profile Radius (r_a). For mathematical modeling purposes, the Half-cone Angle (γ) can be replaced by Roller Plane Height (h), facilitating the equationing of geometrical misalignments (Raizer and Dedini, 2009; Raizer, 2010).

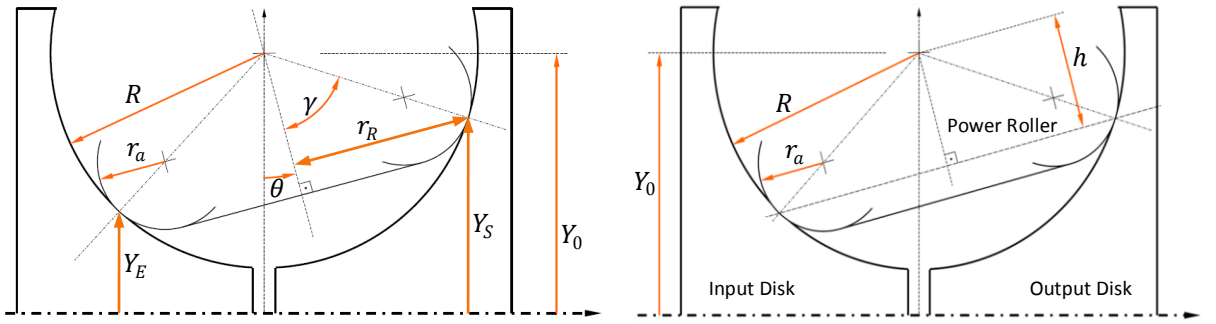

Figure 1. Basic geometric modeling of T-CVT cavity.

2.1. Geometric Modeling of T-CVT

The theoretical gear ratio, also called Ideal Transmission Ratio (Ideal TR, RT_{Tid}), depends on the input contact point height (Y_E) and output contact point height (Y_S), as shown in Eq. 1. Equations 2, 3 and 4 (Raizer and Dedini, 2009) are used to evaluate the contact points positions for any configuration of tilt angle (θ) or misalign angles (α and β).

$$RT_{Tid} = \frac{Y_E}{Y_S} \tag{1}$$

$$Y_E = Y_0 - \frac{h\cdot cos\,\beta\cdot cos\,\theta + (cos\,\alpha\cdot sin\,\theta\cdot cos\,\beta - sin\,\alpha\cdot sin\,\beta)\cdot\sqrt{R^2\cdot G - h^2}}{G} \tag{2}$$

$$Y_S = Y_0 - \frac{h\cdot cos\,\beta\cdot cos\,\theta - (cos\,\alpha\cdot sin\,\theta\cdot cos\,\beta - sin\,\alpha\cdot sin\,\beta)\cdot\sqrt{R^2\cdot G - h^2}}{G} \tag{3}$$

$$G = 1 - cos^2\,\alpha\cdot sin^2\,\beta - sin^2\,\alpha\cdot cos^2\,\beta\cdot sin^2\,\theta - 0{,}5\cdot sin\,2\alpha\cdot sin\,2\beta\cdot sin\,\theta \tag{4}$$

Besides providing a Side-slip condition, α and β changes the effective geometry of the contact. The hypothesis adopted was that the angular gap between the planes doesn't change the elliptical geometry of the contact, and thus the effective radius of the roller surface in the direction of one of the main planes of the disk can be estimated by a weighted average of the principal radii of surfaces, function of the misalignment between the roller and the disk rolling direction (Φ). And so, the principal radii of curvature from the surfaces, written in the disc contact reference, can be written as shown in Eq.5 and Eq.6. Equation 7 and Eq. 8 contains the procedure to calculate the Φ value for the input contat (Φ_E) and for the output contact (Φ_S), using the information from the coordinate transformation matrices arranged in Eq.9, Eq.10, Eq.11 and Eq.12 (Raizer, 2010).

$$\begin{bmatrix} R_{Dx} \\ R_{Dy} \end{bmatrix}_i = R\cdot\begin{bmatrix} Y_i/(Y_0 - Y_i) \\ -1 \end{bmatrix} \tag{5}$$

$$\begin{bmatrix} R_{Rox} \\ R_{Roy} \end{bmatrix}_i = \begin{bmatrix} cos^2\,\Phi_i & sin^2\,\Phi_i \\ sin^2\,\Phi_i & cos^2\,\Phi_i \end{bmatrix}\cdot\begin{bmatrix} r_R \\ r_a \end{bmatrix} = \begin{bmatrix} cos^2\,\Phi_i & sin^2\,\Phi_i \\ sin^2\,\Phi_i & cos^2\,\Phi_i \end{bmatrix}\cdot\begin{bmatrix} \sqrt{R^2 - h^2} \\ r_a \end{bmatrix} \tag{6}$$

$$\begin{bmatrix} cos\,\Phi_E & -sin\,\Phi_E & 0 \\ sin\,\Phi_E & cos\,\Phi_E & 0 \\ 0 & 0 & 1 \end{bmatrix} = [S_{CD}]_E\cdot[S_{D0}]_E\cdot([S_{CR}]_E\cdot[S_{R0}])^{-1} \tag{7}$$

$$\begin{bmatrix} cos\,\Phi_S & sin\,\Phi_S & 0 \\ -sin\,\Phi_S & cos\,\Phi_S & 0 \\ 0 & 0 & 1 \end{bmatrix} = [S_{CD}]_S\cdot[S_{D0}]_S\cdot([S_{CR}]_S\cdot[S_{R0}])^{-1} \tag{8}$$

$$[S_{D0}]_E = \begin{bmatrix} 1 & 0 & 0 \\ 0 & 1 & 0 \\ 0 & 0 & 1 \end{bmatrix};\ [S_{D0}]_S = \begin{bmatrix} -1 & 0 & 0 \\ 0 & 1 & 0 \\ 0 & 0 & -1 \end{bmatrix} \tag{9}$$

$$[S_{R0}]^{-1} = \begin{bmatrix} cos\,\alpha & 0 & sin\,\alpha \\ 0 & 1 & 0 \\ -sin\,\alpha & 0 & cos\,\alpha \end{bmatrix}\cdot\begin{bmatrix} cos\,\theta & -sin\,\theta & 0 \\ sin\,\theta & cos\,\theta & 0 \\ 0 & 0 & 1 \end{bmatrix}\cdot\begin{bmatrix} 1 & 0 & 0 \\ 0 & cos\,\beta & -sin\,\beta \\ 0 & sin\,\beta & cos\,\beta \end{bmatrix} \tag{10}$$

$$[S_{CR}]_i = \begin{bmatrix} -\sin\varphi_i & 0 & -\cos\varphi_i \\ -(h/R)\cos\varphi_i & \sqrt{R^2-h^2}/R & (h/R)\sin\varphi_i \\ -(r_R/R)\cos\varphi_i & h/R & \left(\sqrt{R^2-h^2}/R\right)\sin\varphi_i \end{bmatrix} \tag{11}$$

$$[S_{CD}]_i = \frac{1}{R}\begin{bmatrix} 0 & 0 & R \\ (Y_0 - Y_i) & |X_i| & 0 \\ -|X_i| & (Y_0 - Y_i) & 0 \end{bmatrix} \tag{12}$$

The angle φ_i (φ_E for the input contact and φ_S for the output contact) is the angular position of the point of contact written in the Roller coordinate system, and is given by Eq.13 as a function of the transformation matrix from the global coordinate system to the roller coordinate system (S_{R0}), the geometric parameters (R, Y_0 and h) and the contact point position (X_i and Y_i).

$$\begin{bmatrix} \cos\varphi_i \\ 0 \\ -\sin\varphi_i \end{bmatrix} = \frac{1}{\sqrt{R^2-h^2}} \cdot \left([S_{R0}] \cdot \begin{bmatrix} X_i \\ Y_i - Y_0 \\ 0 \end{bmatrix} + \begin{bmatrix} 0 \\ h \\ 0 \end{bmatrix} \right) \tag{13}$$

2.3. Modeling of lubrication and contact forces

Considering a "quasi-identical" problem, or in other words, a situation where the bodies in contact have nearly the same elastic properties, the contact problem can be solved independently for the tangential efforts and for the normal efforts (Forti, 2003), thus facilitating their resolution. Despite the flow of lubricant slightly change the pressure profile in the contact area (Nonato, 2009), it is common to use the hertzian contact resolution directly as a first approach (Attia, 2005; Carbone *et al.*, 2004; Forti, 2003; Nikas, 2002; Zhang *et al.*, 2000). The results of the hertzian contact theory may also be used together with the rolling bearings life prediction models in order to estimate the T-CVT life time with little error (Lee *et al.*, 2004; Nikas, 2002;Coy *et al.*, 1976). The resolution of the hertzian contact problem can be easily found in nowadays bibliographic (Harris and Kotzalas, 2006; Attia, 2005; Carbone *et al.*, 2004; Forti, 2003; Zhang *et al.*, 2000). Figure 2 has information concerning the geometrical modeling of the surfaces near the contact point and the resultant elliptical contact area.

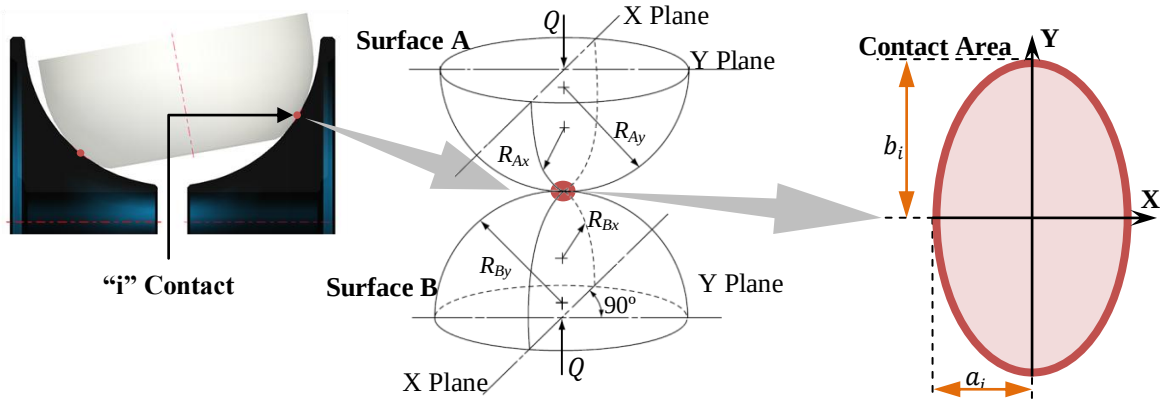

Figure 2. Contact area and local surface geometry.

Assuming a negligible relative velocity due material deformation (on both tangential and normal directions) of the elastic bodies and a nearly constant fluid film thickness, the relative velocity between the roller and the discs for each point of the contact area ($\overrightarrow{V_{Rel}}$), can be written as a function of the Slip and Side-slip velocities (V_{Slip} and $V_{Side\text{-}Slip}$ respectively) and the Spin rotation (ω_{Spin}), as shown on Eq.14 (adapted from *Carbone et al.*, 2004).

$$\overrightarrow{V_{Rel}} = \begin{bmatrix} V_{RelX} \\ V_{RelY} \\ 0 \end{bmatrix} = \begin{bmatrix} V_{Slip} \\ V_{Side-Slip} \\ 0 \end{bmatrix} + \omega_{Spin} \cdot \begin{bmatrix} -y \\ x \\ 0 \end{bmatrix} = \begin{bmatrix} V_{Slip} \\ V_{Side-Slip} \\ 0 \end{bmatrix} + \omega_{Spin} \cdot r \cdot \begin{bmatrix} -b_i \cdot \sin\psi \\ a_i \cdot \cos\psi \\ 0 \end{bmatrix} \tag{14}$$

The Spin rotation (ω_{Spin}) can be calculated using the difference between the angular velocities of the bodies in contact, projected in the normal direction of the contact (Raizer, 2010; Carbone *et al.*, 2004). Equation 15 and Eq.16 have information regarding the calculus of Slip and Side-Slip velocities, already considering the angular misalignment due α and β. With those, V_{Slip} and $V_{Side\text{-}Slip}$ are written as a function of the input disk rotation (ω_E), output disk rotation

(ω_S), roller rotation (ω_{Rolo}), the contact heights (Y_E for input and Y_S for output), roller radius (r_R) and the angular misalignments Φ_E and Φ_S, calculated with the procedure presented in the previous section.

$$\begin{bmatrix} V_{Slip} \\ V_{Side-Slip} \end{bmatrix}_E = Y_E \cdot \omega_E \cdot \begin{bmatrix} 1 \\ 0 \end{bmatrix} - r_R \cdot \omega_{Rolo} \cdot \begin{bmatrix} cos\,\Phi_E \\ sin\,\Phi_E \end{bmatrix} \tag{15}$$

$$\begin{bmatrix} V_{Slip} \\ V_{Side-Slip} \end{bmatrix}_S = r_R \cdot \omega_{Rolo} \cdot \begin{bmatrix} 1 \\ 0 \end{bmatrix} - Y_S \cdot \omega_S \cdot \begin{bmatrix} cos\,\Phi_S \\ sin\,\Phi_S \end{bmatrix} \tag{16}$$

Equation 17 (from Raizer, 2010) relates $\overrightarrow{V_{Rel}}$ and pressure distribution on the contact area with the tangential forces (F_S on the Slip direction and F_{SS} on the Side-slip direction) and the Spin Momentum (normal to the contact area).

$$\begin{bmatrix} F_s \\ F_{ss} \\ M_S \end{bmatrix}_i = a_i b_i \int_0^1 \left(r \cdot \left(\int_0^{2\pi} \frac{\tau_L}{|\overrightarrow{V_{Rel}}|_i} \cdot \left(1 - e^{-\frac{\eta \cdot |\overrightarrow{V_{Rel}}|_i}{\tau_L \cdot H_i}} \right) \cdot \begin{bmatrix} 1 & 0 & 0 \\ 0 & 1 & 0 \\ -b_i\,sin\,\psi & a_i\,cos\,\psi & 0 \end{bmatrix} \cdot \overrightarrow{V_{Rel}}_i d\psi \right) \right) dr \tag{17}$$

The quantity τ_L is the limiting shear stress of the lubricant, normally evaluated for a certain value of the oil temperature, and is given by Eq.18, where τ_{L0} is the limiting shear stress at the atmospheric pressure and p is the punctual pressure exerted on the fluid (Hamrock *et al.*, 2004). Equation 19 enables the evaluation of fluid viscosity (η) over the whole contact region, according to the Roelands model and considering the isothermal contact hypothesis (Carbone *et al.*, 2004). For simplifying purposes, was assumed that the oil film thickness (H_i) is uniform within the contact area, being equal to the film thickness of the contact center (H_c). From Hamrock and Dowson (1981) the H_C formula for hard EHD Lubrication conjunctions is given by Eq.20 (Hamrock *et al.*, 2004).

$$\tau_L = \tau_{L0} + \frac{\partial \tau_L}{\partial p} \cdot p = \tau_{L0} + \zeta \cdot p \tag{18}$$

$$\eta = \eta_0 \cdot \left(\frac{\eta_\infty}{\eta_0} \right)^{1-\left(1+\frac{p}{cp}\right)^{z1}} = \eta_\infty \cdot \left(\frac{\eta_0}{\eta_\infty} \right)^{\left(1+\frac{p}{cp}\right)^{z1}} \tag{19}$$

$$[H_c]_i = \left[2{,}69 \cdot Rx \cdot \left(\frac{V_f \cdot \eta_0}{E_{eq} \cdot Rx} \right)^{0{,}67} \cdot \left(E_{eq} \cdot \frac{z1}{cp} \cdot ln\left(\frac{\eta_0}{\eta_\infty} \right) \right)^{0{,}53} \cdot \left(\frac{Q}{E_{eq} \cdot Rx^2} \right)^{-0{,}067} \cdot (1 - 0{,}61 \cdot e^{-0{,}73k}) \right]_i \tag{20}$$

Where E_{eq} is the equivalent Young Modulus (considering, generically, bodies A and B in contact, with the Young Modules E_A and E_B and Poisson Ratios $\vartheta_A$and ϑ_B, respectively), given by Eq.21, R_x is the equivalent radius of curvature for the contact surfaces at the rolling direction (${R_x}^{-1} = {R_{Ax}}^{-1} + {R_{Bx}}^{-1}$), V_f is the mean fluid velocity, η_0 is the absolute viscosity at the atmospheric pressure, cp is the Pole pressure constant of Roelands viscosity model, η_∞ is the pole viscosity of Roelands viscosity model, Q is resultant normal loading force at the contact and k is the contact ellipticity ($k = a/b$).

$$E_{eq} = 2\left(\frac{(1-{\vartheta_A}^2)}{E_A} + \frac{(1-{\vartheta_B}^2)}{E_B} \right)^{-1} \tag{21}$$

2.2. Modeling of pressure mechanism and bearing loss

A good way to promote contact pressure in the T-CVT's automotive application is a mechanical cam combined with a conical spring disc (Machida and Murakami, 2000). The conical disc spring function is to secure the minimum pressure at the contact point even when the input shaft torque is zero or very small. For the normal range of operation of a T-CVT the loading cam is responsible for the system pressurization, giving a linear relation between the input torque (T) and the axial load (F_a), responsible for the normal loading force at the contact (Q) as seen in Eq.22 and in Fig.3. The axial load (F_a) is equally distributed between the rollers at the toroidal cavity (N_{rc} is the number of rollers per cavity) and multiplied by a factor dependant of the contact inclination (δ).

$$Q_i = \frac{F_a}{N_{rc} \cdot sin\,\delta_i} = \frac{2 \cdot \pi \cdot T}{L_c \cdot N_{rc} \cdot sin\,\delta_i} \tag{22}$$

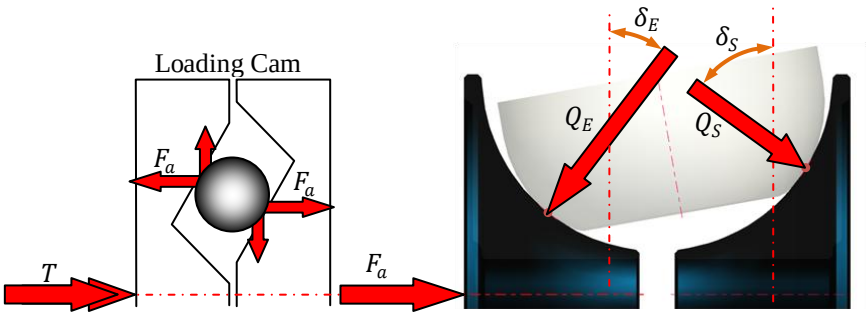

Figure 3. Pressurization of the contacts by a Loading Cam.

At the Roller, the normal contact load Q_E and Q_S are balanced by an axial thrust applied by the roller bearing. In order to estimate torque bearing loss of the power roller bearing the Eq.23 (adapted from Carbone *et al.*, 2004) relates the normal contact loads, projected by the half-cone angle (γ), with T_{BL}. In this equation, Q_E and Q_S are measured in (N) and the torque bearing loss T_{BL} is measured in (Nm).

$$T_{BL} = 4{,}6 \cdot 10^{-5} \cdot [(Q_E + Q_S) \cdot \cos\gamma]^{1{,}03} \tag{23}$$

2.4. Life Modeling

Life prediction models for ball and roller bearings has been used to predict the T-CVT's components life subjected to highly load contacts since Coy *et al.* (1976), due to the similarity of the failure causes. There are four different models to life prediction of constant amplitude and frequency load: Weibull; Lundberg and Palmgren; Ioannidas and Harris; Zaretsky. The basis of all four are described in the work of Zaretsky et al. (2000), as well the origin of Eq.24 (for Weibull model), Eq.25 (for Lundberg and Palmgren model), Eq.26 (for Ioannidas and Harris model) and Eq.27 (for Zaretsky model).

$$L = A\left(\frac{1}{\tau_0}\right)^{\frac{c}{e}}\left(\frac{1}{V}\right)^{\frac{1}{e}} \tag{24}$$

$$L = A\left(\frac{1}{\tau_0}\right)^{\frac{c}{e}}\left(\frac{1}{V}\right)^{\frac{1}{e}}(z_0)^{\frac{h_z}{e}} \tag{25}$$

$$L = A\left(\frac{1}{\tau_0 - \tau_u}\right)^{\frac{c}{e}}\left(\frac{1}{V}\right)^{\frac{1}{e}}(z_0)^{\frac{h_z}{e}} \tag{26}$$

$$L = A\left(\frac{1}{\tau_0}\right)^{c}\left(\frac{1}{V}\right)^{\frac{1}{e}} \tag{27}$$

Where L is contact life, A is material life factor, τ_0 is critical shear stress, V is the stressed volume, z_0 is the depth to maximum critical shear stress, c is the critical shear stress-life exponent, e is the Weibull slope, h_z is the depth exponent and τ_u fatigue limit. Further information about those life models and their exponents can be found on the work of Zaretsky *et al.* (2000). Coy *et al.* (1976) reasoned that the stressed volume may be estimated using the elliptical contact semi-width (b), z_0 and the rolling track length (l), as shown on Eq.28. To evaluate the final surface damage due multiple loading and variable loading and speed, the Miner rule (also called as Lundberg and Miner rule, or Linear damage rule) was used to estimate the life for each component (L_{DE} for the input disk, L_{DS} for the output disk and L_R for the roller). The procedure to implement the Miner rule can be found at Zaretsky (1997). Equation 29 (adapted from Dedini, 1985) was used to achieve an equivalent system life time (L_S).

$$V = b \cdot z_0 \cdot l \tag{28}$$

$$L_S = [N_c \cdot ({L_{DE}}^{-e} + {L_{DS}}^{-e} + N_{rc} \cdot {L_R}^{-e})]^{-1/e} \tag{29}$$

3. LONGITUDINAL VEHICLE DYNAMICS

The objective of this work is to evaluate the impact of misalignments on the geometric construction of T-CVT on its performance, considering an automotive application.

For that purpose, a longitudinal vehicle dynamic model were implemented considering the external forces that oppose to the vehicle motion ($\Im$, as a function of the aerodynamic drag, rolling resistance and grading resistance), given by Eq.30 (adapted from Gillespie,1992; Jazar, 2008), and a simplified model for the vehicle powertrain (described in Tab.1, along with the Eq.31 to Eq.48). Additional data of the values used in this simulation are displayed at Tab.2.

$$\Im = \frac{1}{2} \cdot \rho \cdot A_{fCar} \cdot C_D \cdot (V_{Car} + V_{ven})^2 + \left(sin\,\delta_{pi} + \left(fr_0 + fr_1 \cdot {V_{Car}}^2\right) \cdot cos\,\delta_{pi}\right) \cdot M_{Car} \cdot g \quad (30)$$

Where de ρ is the air density (assumed 1,2258kg/m³), V_{Car} is the vehicle speed, V_{ven} is the wind velocity, δ_{pi} is the street inclination, g is the gravitational acceleration (9,81m/s²), fr_0 and fr_1 are constants of the rolling resistance model ($fr_0 = 0{,}015$ and $fr_1 = 7 \cdot 10^{-6} s^2 m^{-2}$, from Jazar, 2008).

Table 1. Modeling of the powertrain Sub-Systems (Raizer, 2010).

Sub-System	Speed Ratios Equation	Nº	Torque and Strength Ratios Equation	Nº
Wheels	$r_w \cdot \omega_9 = V_{Car}$	(31)	$\Im = \frac{T_9 - 4 \cdot I_w \cdot \dot{\omega}_9}{r_w} - M_{Car} \cdot \dot{V}_{Car}$	(32)
Brakes	$\omega_8 = \omega_9$	(33)	$T_9 = T_8 - T_F$	(34)
Differential	$RT_d \cdot \omega_7 = \omega_8$	(35)	$T_8 = \frac{T_7 \cdot \varepsilon_d}{RT_d}$	(36)
Driveshaft	$\omega_6 = \omega_7$	(37)	$T_7 = T_6 \cdot \varepsilon_E - I_T \cdot \dot{\omega}_6$	(38)
Clutch	$\omega_5 \cdot (1 - Cr_{emb}) = \omega_6$	(39)	$T_6 = T_5 - C_{embE} \cdot \omega_5$	(40)
Output Reduction	$\omega_5 = RT_S \cdot \omega_4$	(41)	$T_5 = \frac{T_4 \cdot \varepsilon_{tS}}{RT_S}$	(42)
Toroidal Cavities	$\omega_4 = RT_T \cdot \omega_3$	(43)	$T_4 = \frac{T_3 \cdot \varepsilon_{tT}}{RT_T}$	(44)
Input Reduction	$\omega_3 = RT_E \cdot \omega_2$	(45)	$T_3 = \frac{T_2 \cdot \varepsilon_{tE}}{RT_E}$	(46)
Engine	$\omega_2 = \omega_{Eng}$	(47)	$T_2 = T_{Eng} - I_{eng} \cdot \dot{\omega}_{Eng}$	(48)

Table 2. Data for simulation of the vehicle equipped with CVT (Raizer, 2010; Genta, 1997).

Property	Value	Property	Value
Vehicle Frontal Area, 'A_{fCar}'	$2{,}3m^2$	Differential TR, 'RT_d'	0,2053
Aerodynamic Drag Coefficient, 'C_D'	0,33	Differential Efficiency, 'ε_d'	0,95
Vehicle Total Mass, 'M_{Car}'	$1130kg$	Gearbox-Type	CVT
Tire effective radius, 'r_w'	$0{,}29m$	TR of adequation, 'RT_{adq}'	0,54110
Equivalent Wheel Inertia, 'I_w'	$0{,}4kg.m^2$	Input Reduction TR, 'RT_S'	0,72434
Equivalent Driveshaft Inertia 'I_T'	$0{,}05kg.m^2$	Input Reduction efficiency, 'ε_{tS}'	0,97
Equivalent Engine Inertia, 'I_{eng}'	$0{,}085kg.m^2$	Input Reduction TR, 'RT_E'	0,74697
Driveshaft efficiency, 'ε_E'	0,99	Input Reduction efficiency, 'ε_{tE}'	0,97
Clutch dissipation coefficient, 'C_{embE}'	$0{,}02\,N.m.s/rad$	Cavity Minimum TR, 'RT_{Tmin}'	0,4328
Traction shaft	Front	Cavity Maximum TR, '$RT_{Tmáx}$'	2,3103

The total brake torque (T_F) and the clutch slip rate (Cr_{emb}) are modeled using Eq.49 and Eq.50 (from Raizer, 2010).

$$T_F = -min\left[\left(T_9 + I_T \frac{\varepsilon_d \cdot \dot{\omega}_9}{{RT_d}^2}\right);\ 0\right] \quad (49)$$

$$Cr_{emb} = 1 - \frac{\omega_6}{max\left[RT_{Tmin} \cdot RT_{adq} \cdot \omega_{fun}\ ; \omega_6\right]} \quad (50)$$

Where: ω_{fun} is the minimum rotational velocity of the ICE's crankshaft and ω_6 is the rotational velocity at the clutch output. The toroidal cavity final TR (RT_T) and efficiency (ε_{tT}) are results from the T-CVT simulation model, and function of the final Slip and Side-slip rate, input torque, the input rotation and the tilt angle (θ). The tilt angle (θ) is determined as a function of the input mechanical power and rotation, using the same methodology described at Raizer (2010). Table 3 contains the geometric parameters and material properties for the simulated T-CVT and Tab.4 contains the lubricant properties tested, both adapted from Carbone *et al.* (2004). Any combination of geometric properties,

material and lubricant could be used, as long as the final result is capable in transmitting the power, torque and rotation required for the external conditions. The vehicle velocity profile, and consequently the acceleration profile, street inclination and wind velocity were determined using the ABNT NBR6601 standard for urban cycles.

Table 3. Geometrical parameters and material properties of the HT-CVT tested (adapted from Carbone *et al.*, 2004).

Parameter	Value	Parameter	Value
Cavity radius 'R'	40,000mm	Number of rollers per cavity, 'N_{rc}'	2
Roller Profile radius, 'r_a'	32,000mm	Number of cavities, 'N_c'	2
Half-cone angle, 'γ'	60º	Fatigue limiting shear stress, 'τ_u'	276MPa
Torus radius, 'Y_0'	65,000mm	Young's Modulus, 'E'	210GPa
Loading Cam Lead, 'L_c'	17,241mm	Poisson ratios, 'ϑ'	0,3

Table 4. Lubricant properties at 99ºC (Carbone et al., 2004).

Property	Value
Absolute viscosity at the atmospheric pressure, 'η_0'	$3{,}25 \cdot 10^{-3}$Pa.s
Limiting shear stress at atmospheric pressure, 'τ_{L0}'	$0{,}02 \cdot 10^{9}$Pa
Limiting shear stress constant, 'ζ'	0,085
Pole pressure constant of Roelands viscosity model, 'cp'	$1{,}96 \cdot 10^{8}$Pa
Pole viscosity of Roelands viscosity model, 'η_∞'	$6{,}31 \cdot 10^{-5}$Pa
Viscosity–pressure index, '$z1$'	0,85

3. RESULTS

Figure 4 has information about the vehicle velocity (V_{Car}) and acceleration ($\dot{V}_{Car}$) during the standard for urban cycle utilized at the simulations, as well a color-coded indicative of the final cavity efficiency. The exactly value of efficiency during the cycle can be estimated comparing the results at Fig.4 with the ones displayed at Fig.5, that contains the efficiency behavior of the T-CVT for three different configurations misalignment angles. It can be observed that these angles have a negative impact on the T-CVT efficiency behavior.

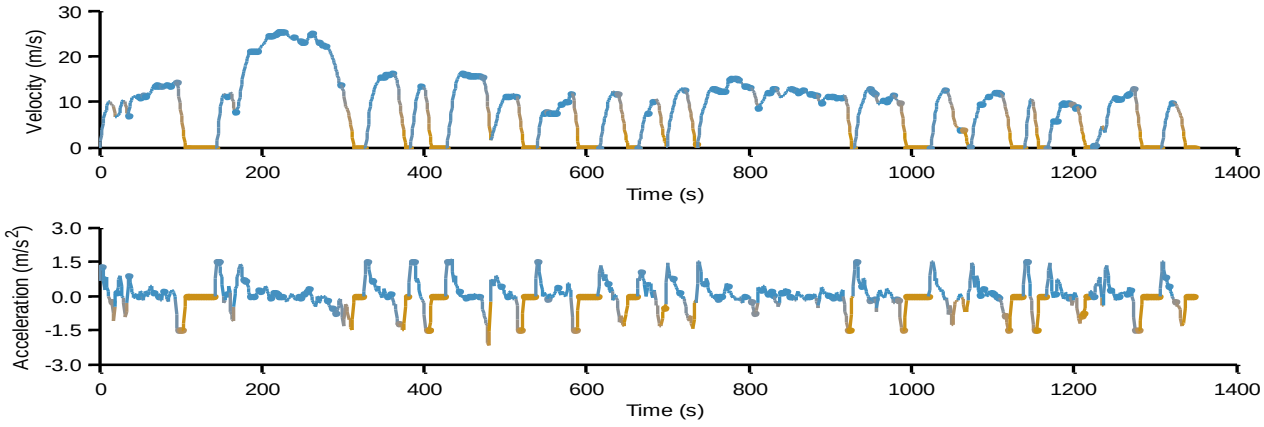

Figure 4. T-CVT's efficiency behavior, vehicle's acceleration and velocity profiles for ABNT NBR6601 urban cycle (Blue: high efficiency, Orange: low Efficiency), with α=0º and β=0º.

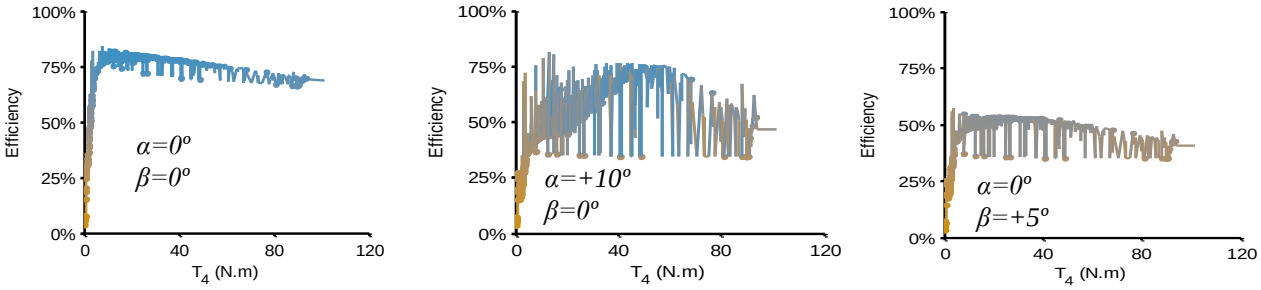

Figure 5. Efficiency behavior of the toroidal cavity as a function of the cavity output torque T_4 (Blue: high efficiency, Orange: low Efficiency).

The sensitivity of the equivalent system life time (L_S) were analyzed using the central point (α=0º and β=0º) as reference, giving the relative variation of equivalent system life time (ΔL_S) as a function of the misalignment angles, as shown on Fig.6. This procedure avoids the dependency of the analysis from the material life factor A (Nikas, 2002).

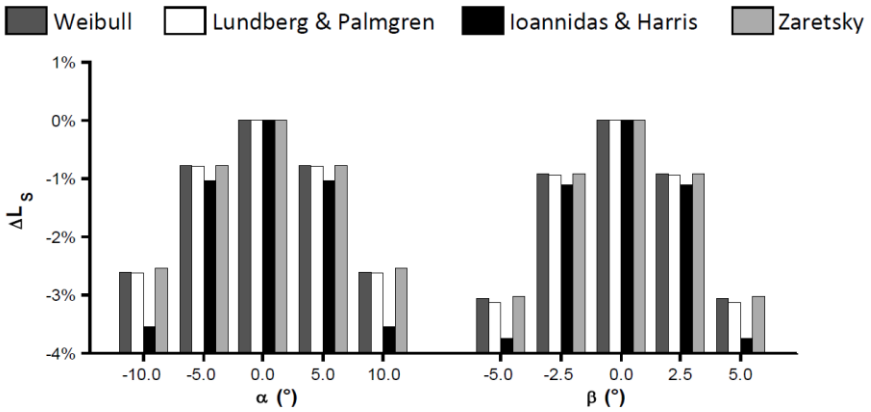

Figure 6. Vehicle acceleration and velocity for ABNT NBR6601 urban cycle.

Figure 7 has results regarding performance parameters, such as: maximum cycle's tilt angle variation ($\Delta\theta_{(max)}$), associated to the overloading effect (Imanishi & Machida, 2000) and the Spin losses (Carbone *et al.*, 2004; Forti, 2003); maximum cycle's toroidal cavity efficiency ($\varepsilon_{tT(max)}$); medium cycle's global sliding coefficient ($cr_{(med)}$) between the output disk and input disk, related to the cavity speed efficiency (defined by Carbone *et al.*, 2004); and the minimum cycle's oil film thickness ($H_{S(min)}$), related to the surface finishing process and, consequently, the cavity manufacturing price (Nikas, 2002). The misalignment angles shows negative impacts over $\varepsilon_{tT(max)}$, $cr_{(med)}$ and $\Delta\theta_{(max)}$, but a positive impact over $H_{S(min)}$, once that the excessive sliding between the surfaces tends to increase their velocity and the lubrication process.

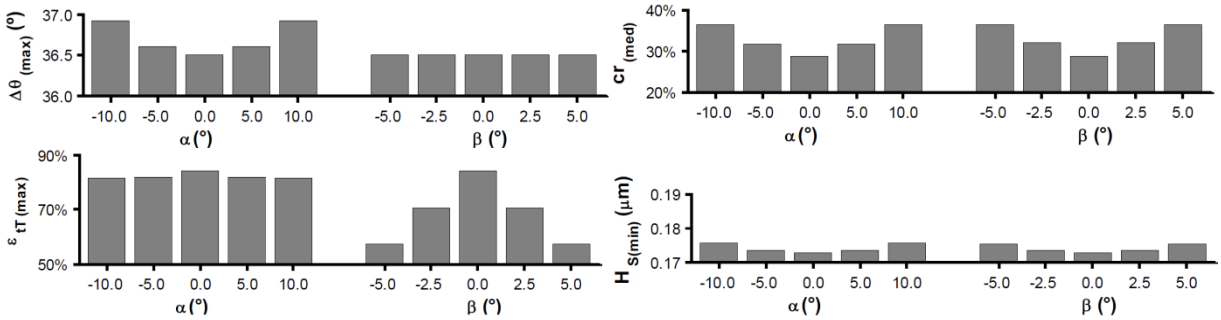

Figure 7. Vehicle acceleration and velocity for ABNT NBR6601 urban cycle.

The efficiency loss and the higher sliding coefficient affects the system capacity of optimize the ICE operation. Figure 8 shows the optimum operation lines for the theoretical engine used at the simulation process, together with the ICE utilization incidence results for three configurations of misalignment angles. It can be observed that, with

misalignments, there is some incidence outside the engine operation lines. It means that, for those points and configuration, the engine is not capable of delivering enough power and torque.

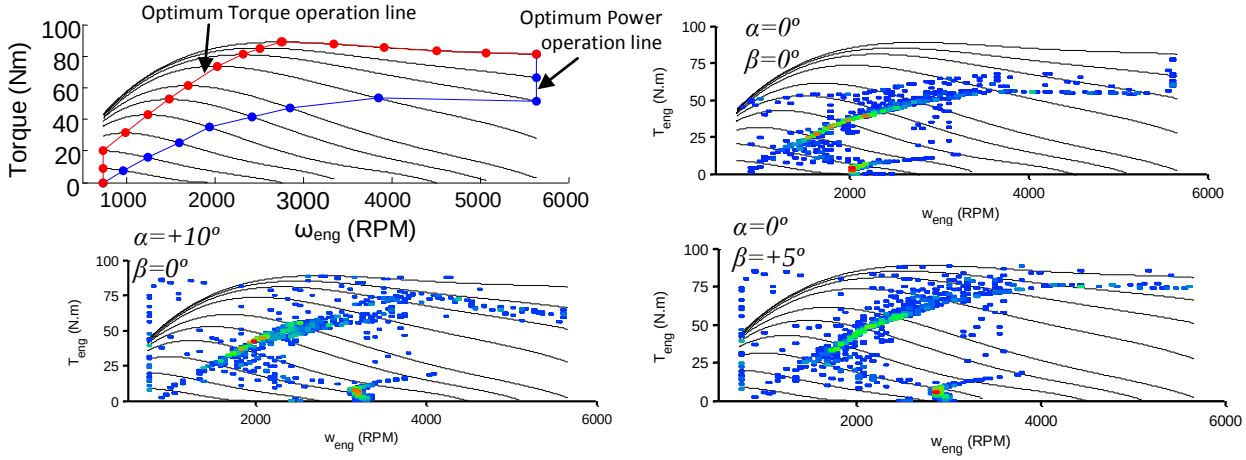

Figure 8. Reference engine operation curves (Raizer, 2010) and the ICE utilization incidence map (Blue: low incidence; Green: medium incidence; Red: high incidence).

3. CONCLUSIONS

The authors conclude that any level of misalignment at the roller axis is prejudicial to the system performance. Some works (Machida & Murakami, 2000) reports the utilization of misalignments and side-slip forces as roller inclination control. So, the maximum values of those angles must be pondered and chosen according to the cost and efficiency compromise.

The proposed methodology is sufficient to predict the T-CVT general behavior, and thus enabling optimization methods based on a project geometric variation. The current mathematical model can utilize data from any real powertrain configuration that utilizes a T-CVT, but it is recognized that it can be refined, upgraded and adjusted in order to retrieve more accurate mathematical information.

4. ACKNOWLEDGEMENTS

The authors would like to thank BOSCH, UNICAMP, CAPES, CNPQ and CTI for the support and help.

5. REFERENCES

Attia, N.A., 2005 "Predicting the Life Contact for Half Toroidal Continuously Variable Transmission." Information technology Journal, 222-227, 2005.

Coy, John J.; Loewenthal, S.H.; Zaretsky, E.V., 1976 "Fatigue life analysis for traction drives with appliation to a toroidal type geometry.", Nasa Technical Note, D-8362, pp:1-31.

Dedini, F.G., 1985 "Projeto e Otimização de uma Transmissão Planetária por Rolos de Tração.", M.Sc. Dissertation, FEM-UNICAMP, Campinas-SP, Brazil.

Forti, A.W., 2003 "Estudo Teórico Experimental de Parâmetros de Projeto de uma Transmissão Continuamente Variável por Tração Tipo Esfera Cone.", PhD. Thesis, FEM-UNICAMP, Campinas-SP, Brazil.

Genta, G., 1997 "Motor Vehicle Dinamics – Modelling and Simulation", World Scientific Publishing Co. Pte Ltd, Singapore, ISBN 9810229119.

Gillespie, T.D., 1992 "Fundamentals of Vehicle Dynamics." Society of Automotive Engineers, Inc. 400 Commonwealth Drive. Warrendale, PA 15096-0001, 1992, ISBN 1-56091-199-9.

Hamrock, B.J., Schmid, S.R., Jacobson, B.O., 2004 "Fundamentals of Fluid Film Lubrication", 2ºEd, Marcel Dekker Inc., New York, 2004, ISBN: 0-8247-5371-2.

Harris, Tedric A.; Kotzalas, Michael N., 2006 "Rolling Bearing Analysis: Essential Concepts of Bearing Technology." CRC Press, Taylor & Francis Group, 5ª ed, 2006, ISBN 978-0-8493-7183-7.

Imanishi, T., Machida, H., 2000 "Development of the POWERTOROS UNIT Half-Toroidal CVT (2) – Comparison between Half-Toroidal and Full-Toroidal CVTs.", NSK Thecnical Journal, n.10, abr. 2001.

Jazar, R.N., 2008 "Vehicle Dynamics: Theory and Application.", Springer, Science+Business Media, LLC, 2008, ISBN 978-0-387-74243-4

Lee, A.P., Newall, J.P., Goto, M., Misada, Y., Ono, Y., 2004, "Experimental Validation of Full Toroidal Fatigue Life." Proceedings of the CVT 2004 Conference - September 23/25, 2004 - San Francisco, USA. 04CVT-21.

Machida, H., Murakami, Y., 2000 "Development of the POWERTOROS UNIT Half Toroidal CVT.", NSK Thecnical Journal, n.9, out. 2000.

Nonato de Paula, F., 2009, "Modelo Dinâmico para o Contato em Mancais de Elementos Rolantes Sujeito à Lubrificação Elastohidrodinâmica.", M.Sc. Dissertation, FEM-UNICAMP, Campinas-SP, Brazil.

Nikas, G.K., 2002 "Fatigue Life and Traction Modeling of Continuously Variable Transmissions.", Journal of Tribology, Transactions of the ASME, v.124, pg.689-698, Oct. 2002.

Raizer, B. and Dedini, F.G., 2009 "Modeling and cinematic analysis of toroidal CVTs: influence of the geometric parameters in performance.", Proceedings of 20th International Congress of Mechanical Engineering (COBEM 2009), Gramado-RS, Brazil. ABCM, 2009. v. COB09. p. 1-8.

Raizer, B. 2010 "Modelagem Modelagem e Análise Cinemática de CVT's Toroidais: Influência dos parâmetros geométricos no desempenho.", M.Sc. Dissertation, FEM-UNICAMP, Campinas-SP, Brazil.

Tenberge, P., Möckel, J., 2002 "Toroidal CVT with compact roller suspension." VDI-Berichte, nº1709, p.623-637.

Zaretsky, E.V., 1997 "Palmgren Revisited – A Basis for Bearing Life Prediction", Nasa Technical Memorandum, NASA/TM 1997-107440

Zaretsky, E.V., Poplawski, J.V., Miller, C.R., 2000 "Rolling Bearing Life Prediction — Past, Present, and Future", Nasa Technical Memorandum, NASA/TM 2000-210529

6. RESPONSIBILITY NOTICE

The following text, properly adapted to the number of authors, must be included in the last section of the paper: The author(s) is (are) the only responsible for the printed material included in this paper.